ChemComm

Waveguiding properties of perylene microcrystals synthesized by retarding the growth along pi-stack direction

Journal:	*ChemComm*
Manuscript ID	CC-COM-12-2020-008094.R1
Article Type:	Communication

COMMUNICATION

Waveguiding Properties of Perylene Microcrystals Synthesized by Retarding the Growth along π-Stack Direction

Received 00th January 20xx,
Accepted 00th January 20xx

Dorothy K. Jones,[a‡] Che-Hsuan Cheng,[b‡] Zidong Li,[b] Xinran Zhang ,[c] Parag B. Deotare,*[d] and Nagarjuna Gavvalapalli*[a]

DOI: 10.1039/x0xx00000x

Selective, hard to realize growth retardation of the π-stacking direction over the edge-packing direction is achieved in perylene microcrystals using an aryl amphiphile. The perylene microcrystals grow predominantly along the edge-packing direction resulting in novel and hitherto unknown perylene square rods. The rods show exciton-polariton waveguiding along the rod axis even though it corresponds to pure edge-packing of the molecules, which is unprecedented in organic microcrystals.

Organic π-conjugated microcrystals (MCs) are useful as waveguides, photo-detectors, chemical sensors, solid-state lasers, logic operators, and multiplexers.[1-11] Waveguiding direction, emission intensity, lasing threshold, and optical losses depend on molecular arrangement along different crystal growth directions.[12-19] Thus, there has been a long-standing interest in altering the crystal growth process to gain control over the π-conjugated MC growth and shape control. Most of the reported crystal growth processes involve crystal growth along the strong π-stacking interaction direction.[20] Therefore, controlling the π-stacking interactions during MC growth is key to alter the crystal growth and shape control.

Several strategies, including alkyl amphiphiles, have been used to alter the organic microcrystal growth processes and generate microcrystals of different shapes. However, most of the reported crystal growth processes involve growth along the strong π-stacking interaction direction. This is because the interactions between alkyl amphiphiles and organic MC π-facet (*alkyl hydrophobe-MC facet* interactions) are not strong enough to disrupt the strong π-π stacking interactions between organic π-conjugated molecules and significantly alter the growth rate of π-stacking direction.

Herein, we show that a biphenyl amphiphile morphology director (MoD) selectively retards the perylene MC growth along the strong π-stacking interaction direction compared to that of weak edge-packing interactions direction (Scheme 1). The MoD significantly altered the perylene growth process compared to the previously reported perylene growth mode. Such a selective retardation of π-stack growth direction over edge-packing direction is hard to realize and to the best of our knowledge not has been reported so far. The MoD resulted in perylene square rod MCs with ca.87% {0 1 1} facet surface area. On the contrary, {0 1 1} facet is not found on the plates grown using conventional alkyl amphiphile CTAB (cetyl trimethylammonium bromide. Higher percent surface area of the {0 1 1} facets results in enhanced coupling between the incident light and lower energy transitions in the square rods compared to the plates. Perylene rods show exciton-polariton waveguiding along the pure molecular edge-packing direction, which is unprecedented in organic microcrystals.

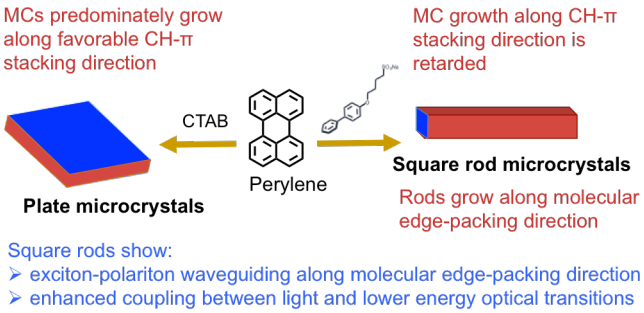

Scheme 1: Difference in the CH-π growth direction in perylene square rod vs. plate microcrystals.

The biphenyl MoD was synthesized in one step via the nucleophilic addition of 1,4-butane sultone to the 4-hydroxybiphenyl (Scheme S1). The perylene MCs were prepared via the reprecipitation method: perylene in THF was rapidly injected into a biphenyl amphiphile aqueous solution. After 24 hours, the resultant solutions were centrifuged and sonicated repeatedly in fresh water to remove the amphiphile and isolate the MCs. The morphology of the MCs was determined using scanning electron microscopy (SEM). This procedure produced well-defined perylene square rod-shaped MCs (Figure 1A) with high shape yield (94%), which were found to be 0.88 ± 0.14 μm in length and 0.27 ± 0.04 μm wide, with a

[a] *Department of Chemistry and Institute of Soft Matter Synthesis and Metrology, Georgetown University, 3700 Ost NW, Washington, D.C. 20057. Email: ng554@georgetown.edu*
[b] *Department of Materials Science and Engineering, University of Michigan, Ann Arbor, Michigan, 48109.*
[c] *Department of Physics and Institute of Soft Matter Synthesis and Metrology, Georgetown University, 3700 Ost NW, Washington, D.C. 20057.*
[d] *Department of Electrical and Computer Engineering, University of Michigan, Ann Arbor, Michigan, 48109.*
‡These authors contributed equally
†Electronic Supplementary Information (ESI) available: See DOI: 10.1039/x0xx00000x

polydispersity in both the length and width of 16% (Figure S1). For comparison, perylene plates (Figure S2) were grown in an aqueous solution of CTAB following the reported protocols.[15] The plates are on average 5.7 ± 2.3 µm long and 5.5 ± 2.4 µm wide (Figure S3).

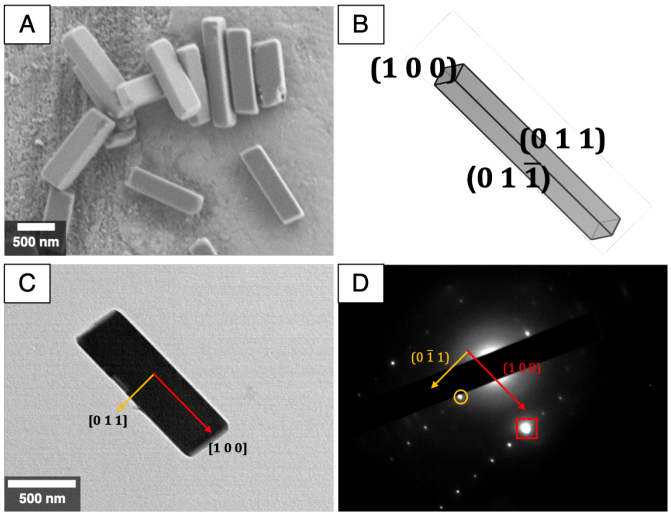

Figure 1 (A) SEM image of perylene rods; (B) cartoon of the rods showing the different exposed facets (C) TEM image of perylene rod and (D) the corresponding selected area diffraction pattern

Transmission mode PXRD patterns of both the square rods and square plates are the same and match well with the α-polymorph (P21/c space group) of perylene (Figure S4). The reflection mode PXRD patterns were also recorded (Figure 2), and the dominant observed facets were determined using relative intensities of the peaks. Based on the PXRD results the plates are bound on the top and bottom by the {1 0 0} faces, which is in agreement with previously reported[13, 15, 16, 21, 22] results that are based on SAED measurements. Interestingly, in the case of the square rods, the relative intensity of the (1 0 0) peak is lower than that of the (0 1 1) peak in the reflection mode PXRD (Figure 2), indicating that the rods have an abundance of the (0 1 1) surface exposed. The SAED pattern of the rods (Figure 1C-D) confirms that the rods are bound on

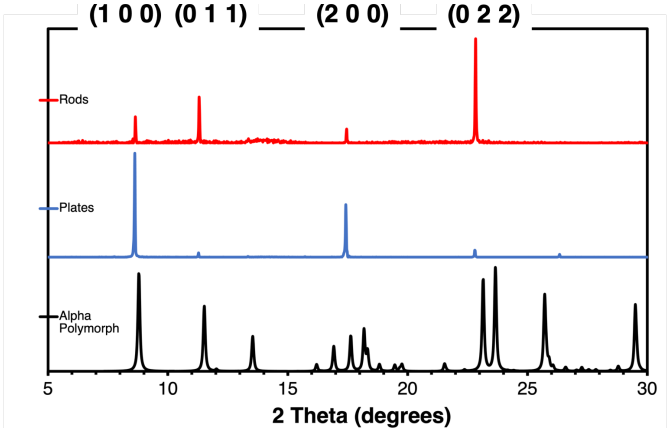

Figure 2 Reflection mode PXRD of perylene MCs and the calculated pattern of α phase.

four sides by the {0 1 1} family of faces, and the rod-tips are bound by the {1 0 0} family of faces. This indicates that the amphiphile hindered growth of the {0 1 1} facets and facilitated the MC growth along the [1 0 0] direction, thereby flipping the observed facet growth in the square plates. The observation of the square rod shaped MC morphologies and the abundant {0 1 1} family of facets on the MC surfaces is hitherto unknown for perylene. Previous reports have shown that the ribbon and plate shape perylene MCs are mostly bound by the {1 0 0}, {0 1 0} or {0 0 1} families of faces.[13, 15, 16, 21, 22] The growth morphology of theoretically generated crystals using the Vesta software match well with the experimentally observed morphologies, including the angles between the facets (Figure S5), which further corroborates our facet indexing.

Growth and equilibrium morphologies (Figure S6) of perylene as well as the surface and attachment energies of the morphologically important facets were calculated using Materials Studio[23] (Table S1). A facet with a higher (or lower) magnitude of E_{hkl}^{attach} is called a higher (or lower) energy facet. Under typical growth conditions, crystals are formed by the rapid growth of higher energy facets to minimize surface area and therefore generate thermodynamically stable equilibrium morphologies that are bound by lower energy facets.[14, 24-26] This is the case when perylene MCs are grown in the presence of CTAB and the resulting perylene plates are bound by the lowest energy {1 0 0} facets.[13, 15, 16, 21, 22] The biphenyl MoD exhibits strong π-stacking interactions with the {0 1 1} facets (CH-π stacking direction), stabilize them and retard their growth, thereby resulting in square rods. Since the growth along the CH-π stacking directions is retarded, the surface area of the facets orthogonal to these directions, {0 1 1} facets, is higher in the resultant MCs (ca. 87% surface area). Structural characterization confirms that no new polymorphs are formed in the presence of amphiphile, thus the different morphologies obtained are due to variations in how the amphiphile interacts with the growing MC facets of perylene α-polymorph. The MCs are centrifuged and are stored as powders for further characterization.

In order to understand the impact of the high surface area of these otherwise generally low surface area CH-π stacking {0 1 1} facet on the photophysical properties of perylene, UV-vis absorption, excitation and emission spectra of the MCs suspended in water were recorded (Figure 3). The peak around 480 nm (Figure 3A and Figure S7) is due to excitonic absorption[27, 28] whereas the peaks above 500 nm are due to scattering. In order to confirm this, the excitation spectra of the MCs were recorded. The peaks seen in the absorbance spectra were also observed in the excitation spectra (Figure 3B), with the exception of peaks around 575 nm confirming that these low-energy broad peaks are due to scattering.

The intensities of lower energy transition peaks ca. 430 and 470 nm are higher for the square rods compared to the plates (Figure 3A-B). The absorption spectrum of square rods is mostly due to the abundant {0 1 1} surfaces while the contribution from the {1 0 0} surfaces is negligible. On the other hand, in the case of plates, the dipoles are oriented orthogonal to the plate {1 0 0} surface in plates (Figure S8). The relative orientation between the induced molecular dipoles and the electric field vector of the incident light is

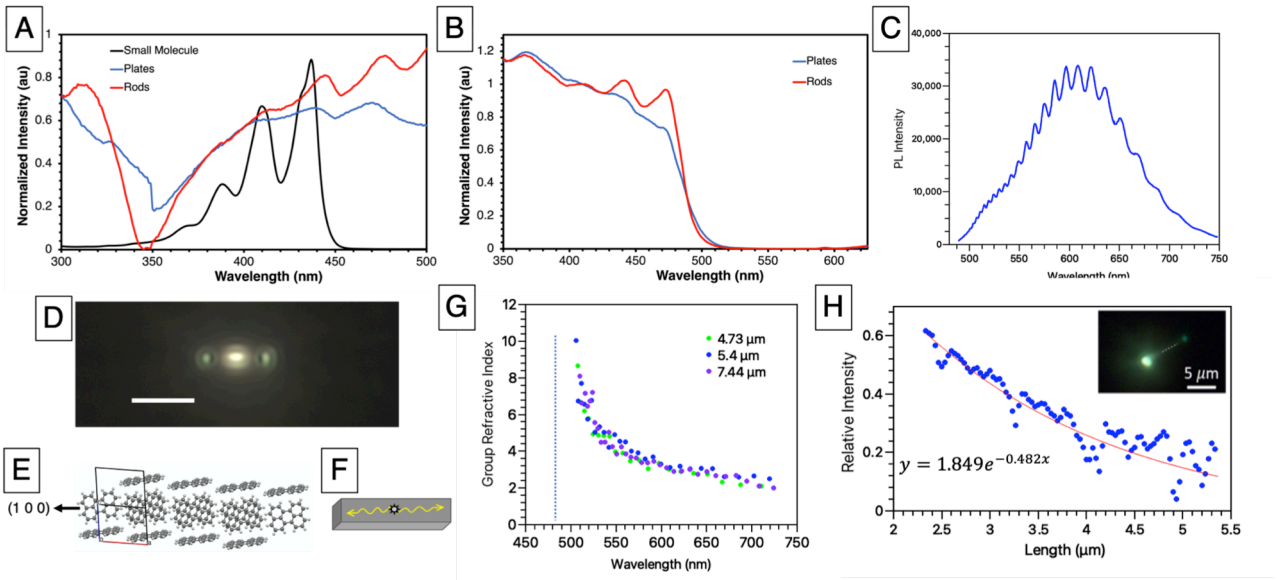

Figure 3: (A) UV-vis adsorption spectra; (B) excitation spectra of the perylene MCs suspended in water (black is the perylene small molecule in THF); (C) PL from one end of the rod showing Fabry-Perot oscillations; (D) Fluorescence microscopy image showing a perylene rod excited with a 450 nm laser (scale bar = 5 µm) waveguiding along the [1 0 0] direction, (E) perylene crystal packing showing the edge-to-edge packing along the [1 0 0] direction; (F) waveguiding direction in the rod; (G) Estimation of group refractive index based on (c) for rods of different lengths. The dashed line denotes the excitonic absorption. (H) Estimation of propagation loss based on light scattering along the length on the rod. The scattering profile represents the dashed line in the inset.

known to control the UV-vis absorption spectrum of the crystals.[29-31] The perylene dipole moment is along the long axis of the molecule.[16, 28, 32] The enhanced intensity of the lower energy transitions in the square rods is due to the non-orthogonal coupling between electromagnetic field vectors and dipoles (Figure S8 and S9). The emission spectra of the two different shaped MCs look almost identical to each other (Figure S10), and are significantly red-shifted relative to the emission of the perylene small molecule.

Next, the waveguiding behaviour of square rods was studied to determine if the light is guided only along the rod axis (along perylene edge-to-edge stacking direction [1 0 0]) to the tips and/or to the rod four faces (along the CH-π stacking direction [0 1 1]). To investigate the waveguiding properties, MCs were grown using modified growth conditions (Figure S11) to generate longer rods of 5-10 µm in length and 1 µm in width. The longer rods have similar PXRD peak pattern as smaller rods (Figure S11) indicating that there is no structural difference between them. Interestingly, the perylene rods emit from both tips when excited (450 nm cw laser) at the middle of the rod (Figure 3D-F). The emission spectra from the rod tips show Fabry-Perot (FP) oscillations (Figure 3C) and confirm active waveguiding in the rods. Since the size of the laser spot is similar to the width of the rod, it was difficult to determine if the light is guided to the side faces.

The FP oscillation in rods are analysed further to understand the active waveguiding mechanism in the perylene rods. The free spectral range ($\Delta\lambda$) of a cavity with a separation (L) between the mirrors is given by the equation $\Delta\lambda = \lambda^2/2Ln_g$, where λ is the peak wavelength, $n_g = n - \lambda(\frac{dn}{d\lambda})$ is the group refractive index,[1, 3] and L is the cavity length (measured using optical microscope). The estimated group refractive index is shown in Figure 3G. The group index increases significantly for wavelengths approaching the excitonic resonance (dashed line). For wavelengths further away from the resonance, the group index is much lower. This shows that propagation slows down by nearly c/10 (c being speed on ligth in vacuum) near the excitonic resonance. We therefore conclude that the observed phenonmenon is due to strong coupling between exciton and photon, giving rise to an exciton polariton. At longer wavelengths (away from resonance), the polariton has photon characteristics where as near the resonance, the excitonc characteristics are dominant.

Optical loss coefficient along the long axis of the rod is estimated based on the scattered light measured along the rod (dashed line in Figure 3H inset) over twelve samples. The optical loss coefficient in rods is 0.435 ± 0.068 dB/ µm (Figure 3H) and ca. 4 times higher than that of the plates[13]. The edge-to-edge packing direction is generally not a predominant direction for charge and exciton transport in π-conjugated materials.[33, 34] Thus, a slightly higher loss coefficient along the weak edge-packing direction in rods over the CH-π stacking direction in plates is noteworthy.[13] To the best of our knowledge, this is the first example in which exciton-polariton waveguiding is observed along the pure edge-edge stacking (i.e. no partial overlap of molecules) direction.

Recently, it has been shown that organic π-conjugated microcrystals display electro-photo coupling and are useful as field-effect optical waveguides.[35] Access to microcrystals whose long axis coincides with the π-stacking or edge-packing direction will behave differently with the applied voltage and result in different electro-photo coupling behaviour and broaden the use of organic microcrystals in optoelectronic applications. Also, the high surface area of the π-stacking facet on the MC facets will enhance the probability of forming continuous pathways for charges to reach electrodes even if

the MCs are assembled randomly in thin films.[36, 37] Thus the MCs with unconventional growth along edge-packing direction enables materials with atypical but remarkable properties, overcomes the limitations of conventional organic materials and helps to push the frontiers of organic π-conjugated materials.

This work highlights the importance of developing novel aryl amphiphiles to control the growth along the hard to realize, π-stacking direction to enable novel MC growth processes in polyaromatic hydrocarbons. The novel growth processes will result in diverse morphologies that are bound by relatively high energy conducting facets. Also, the MCs grown along the weak edge-packing direction will help to complement our fundamental knowledge on the charge, exciton, and energy transport properties, which is mostly developed from the conventional assemblies that are predominately grown via strong π-stacking interactions.

We thank the Donors of the American Chemical Society Petroleum Research Fund (#58444-DNI7) for partial support of this research. D.K.J. thanks the Clare Boothe Luce foundation. X. Z. thanks Andrea Brothers at the Department of Chemistry, American University for providing TEM training and access.

Conflicts of interest

There are no conflicts to declare

Notes and references

1. Y. L. Yan and Y. S. Zhao, *Adv. Funct. Mater.*, 2012, **22**, 1330-1332.
2. Q. H. Cui, Y. S. Zhao and J. N. Yao, *Adv. Mater.*, 2014, **26**, 6852-6870.
3. Q. Liao, Z. Z. Xu, X. L. Zhong, W. Dang, Q. Shi, C. Zhang, Y. X. Weng, Z. Y. Li and H. B. Fu, *J. Mater. Chem. C*, 2014, **2**, 2773-2778.
4. W. Zhang and Y. S. Zhao, *Chem. Commun.*, 2016, **52**, 8906-8917.
5. M. P. Zhuo, Y. C. Tao, X. D. Wang, Y. C. Wu, S. Chen, L. S. Liao and L. Jiang, *Angew. Chem. Int. Ed.*, 2018, **57**, 11300-11304.
6. J. Clark and G. Lanzani, *Nat. Photonics*, 2010, **4**, 438-446.
7. J. Liu, L. Jiang, J. Shi, C. Li, Y. Shi, J. Tan, H. Li, H. Jiang, Y. Hu, X. Liu, J. Yu, Z. Wei, L. Jiang and W. Hu, *Adv. Mater.*, 2020, **32**, e1906122.
8. L. Catalano, J. Berthaud, G. Dushaq, D. P. Karothu, R. Rezgui, M. Rasras, S. Ferlay, M. W. Hosseini and P. Naumov, *Adv. Funct. Mater.*, 2020, 2003443.
9. M. Annadhasan, A. R. Agrawal, S. Bhunia, V. V. Pradeep, S. S. Zade, C. M. Reddy and R. Chandrasekar, *Angew. Chem. Int. Ed.*, 2020, **59**, 13852-13858.
10. J. M. Halabi, E. Ahmed, L. Catalano, D. P. Karothu, R. Rezgui and P. Naumov, *J. Am. Chem. Soc.*, 2019, **141**, 14966-14970.
11. L. Catalano, P. Commins, S. Schramm, D. P. Karothu, R. Rezgui, K. Hadef and P. Naumov, *Chem. Commun.*, 2019, **55**, 4921-4924.
12. X. Wang, H. Li, Y. Wu, Z. Xu and H. Fu, *J. Am. Chem. Soc.*, 2014, **136**, 16602-16608.
13. Q. Liao, H. Zhang, W. Zhu, K. Hu and H. Fu, *J. Mater. Chem. C*, 2014, **2**, 9695-9700.
14. H. Liu, X. Cao, Y. Wu, Q. Liao, A. J. Jimenez, F. Wurthner and H. Fu, *Chem. Commun.*, 2014, **50**, 4620-4623.
15. Y. Lei, Q. Liao, H. Fu and J. Yao, *J. Phys. Chem. C*, 2009, **113**, 10038-10043.
16. Z. Z. Li, L. S. Liao and X. D. Wang, *Small*, 2018, **14**, 1702952.
17. M. Goel, K. Narasimha and M. Jayakannan, *J. Phys. Chem. B*, 2015, **119**, 5102-5112.
18. X. Han, M. Bag, T. S. Gehan, D. Venkataraman and D. Maroudas, *J. Phys. Chem. C*, 2015, **119**, 25826-25839.
19. N. R. Goud, X. Zhang, J.-L. Brédas, V. Coropceanu and A. J. Matzger, *Chem*, 2018, **4**, 150-161.
20. It is generally agreed that specific pi-stacking interactions do not exist as a distinct intermolecular interaction between closed-shell molecules. See e.g. S. Gimme, *Angew. Chem. Int. Ed.* 2008, **47**, 3430-3434; C. R. Martinez, B. L. Iverson, *Chem. Sci.* 2012, **3**, 2191-2201. However, for convenience, we will refer to the distinct configurations with their distinct interaction energies as pi-stacking and CH-pi stacking interactions.
21. Y. Lai, H. Li, J. Pan, J. Guo, L. Kang and Z. Cao, *Cryst. Growth Des.*, 2015, **15**, 1011-1016.
22. K. Takazawa, *Chem. Phys. Lett.*, 2017, **667**, 284-289.
23. BIOVIA, Dassault Systèmes, Materials Studio, San Diego: Dassault Systèmes, **2019**.
24. B. D. Hamilton, J. M. Ha, M. A. Hillmyer and M. D. Ward, *Acc. Chem. Res.*, 2012, **45**, 414-423.
25. D. Winn and M. F. Doherty, *Aiche Journal*, 2000, **46**, 1348-1367.
26. J. Li, C. J. Tilbury, S. H. Kim and M. F. Doherty, *Prog. Mater. Sci.*, 2016, **82**, 1-38.
27. L. Kang, Z. Wang, Z. Cao, Y. Ma, H. Fu and J. Yao, *J. Am. Chem. Soc.*, 2007, **129**, 7305-7312.
28. T. Rangel, A. Rinn, S. Sharifzadeh, F. H. da Jornada, A. Pick, S. G. Louie, G. Witte, L. Kronik, J. B. Neaton and S. Chatterjee, *Proc. Natl. Acad. Sci. U S A*, 2018, **115**, 284-289.
29. D. A. McQuarrie and J. D. Simon, *Physical Chemistry: A Molecular Approach*, University Science Books, Sausalito, CA, 1997.
30. M. A. Loi, E. da Como, F. Dinelli, M. Murgia, R. Zamboni, F. Biscarini and M. Muccini, *Nat. Mater.* , 2004, **4**, 81-85.
31. J. E. Park, M. Son, M. Hong, G. Lee and H. C. Choi, *Angew. Chem. Int. Ed.*, 2012, **51**, 6383-6388.
32. J. Shi, M. E. Pollard, C. A. Angeles, R. Chen, J. C. Gates and M. D. B. Charlton, *Sci. Rep.*, 2017, **7**, 1812.
33. V. Coropceanu, J. Cornil, D. A. da Silva, Y. Olivier, R. Silbey and J. L. Bredas, *Chem. Rev.*, 2007, **107**, 926-952.
34. J. Mei, Y. Diao, A. L. Appleton, L. Fang and Z. Bao, *J. Am. Chem. Soc.*, 2013, **135**, 6724-6746.
35. G. Zhao, H. Dong, Q. Liao, J. Jiang, Y. Luo, H. Fu and W. Hu, *Nat. Commun.*, 2018, **9**, 4790.
36. R. Li, L. Jiang, Q. Meng, J. Gao, H. Li, Q. Tang, M. He, W. Hu, Y. Liu and D. Zhu, *Adv. Mater.*, 2009, **21**, 4492-4495.
37. G. Giri, S. Park, M. Vosgueritchian, M. M. Shulaker and Z. Bao, *Adv. Mater.*, 2014, **26**, 487-493.

1